Inorganic Chemistry Communications 190 (2026) 116860

Contents lists available at ScienceDirect

Inorganic Chemistry Communications

journal homepage: www.elsevier.com/locate/inoche

Research Article

# Design and biological evaluation of a quinoline-substituted silicon phthalocyanines for photodynamic therapy of endometrial cancer: topoisomerase IIα targeting and apoptosis induction

Gökçe Seyhan [a,b], Yasemin Altun Ali [c,d], Elif Nur Barut [e], Manar M. Amin [f,g], Turgut Keles [h], Suat Sari [i], Baybars Koksoy [j], Can Özgür Yalcin [c], Zekeriya Biyiklioglu [k], Burak Barut [a,*]

[a] Karadeniz Technical University, Faculty of Pharmacy, Department of Biochemistry, Trabzon, Türkiye
[b] Karadeniz Technical University, Graduate School of Health Sciences, Department of Biochemistry (Pharmacy), Trabzon, Türkiye
[c] Karadeniz Technical University, Faculty of Pharmacy, Department of Pharmaceutical Toxicology, Trabzon, Türkiye
[d] İstanbul University, Institute of Graduate Studies in Health Sciences, İstanbul, Türkiye
[e] Karadeniz Technical University, Faculty of Pharmacy, Department of Pharmacology, Trabzon, Türkiye
[f] Karadeniz Technical University, Graduate School of Health Sciences, Department of Pharmacology, Trabzon, Türkiye
[g] University of Khartoum, Faculty of Pharmacy, Department of Pharmacology, Khartoum, Sudan
[h] Recep Tayyip Erdogan University, Central Research Laboratory Application and Research Center, Rize, Türkiye
[i] Hacettepe University, Faculty of Pharmacy, Department of Pharmaceutical Chemistry, Ankara, Türkiye
[j] Bursa Technical University, Department of Chemistry, Bursa, Türkiye
[k] Karadeniz Technical University, Faculty of Science, Department of Chemistry, Trabzon, Türkiye

ARTICLE INFO

*Keywords:*
Endometrial cancer
Photodynamic therapy
Silicon (IV) phthalocyanines
Apoptosis
Topoisomerase II

ABSTRACT

In this study, to discover potentially selective and safe therapeutic candidates for photodynamic therapy (PDT), new quinoline-derived silicon phthalocyanine compounds (8K-C3-D-Si and 8K-C3-D-SiQ) were synthesized, characterized, and their PDT potential was evaluated. The synthesized compounds were characterized using spectroscopic methods such as FT-IR, $^{1}$H NMR, $^{13}$C NMR, MS, and UV–Vis. In photochemical measurements, the singlet oxygen production capacities and photostabilities of the compounds were investigated, and observed that 8K-C3-D-SiQ exhibited a higher effectiveness ($\Phi_{\Delta} = 0.088 \pm 0.009$ for 8K-C3-D-Si and $\Phi_{\Delta} = 0.345 \pm 0.034$ for 8K-C3-D-SiQ). The $IC_{50}$ value of 8K-C3-D-SiQ in the human endometrial cancer cell line (HEC-1B) after 24 h of incubation in the presence of light was found to be 84.18 ± 14.84 nM. In cells treated with 0.1 μM 8K-C3-D-SiQ, late apoptosis was detected at 54.03 ± 3.10% and necrosis at 22.74 ± 5.98% under light exposure. At the molecular level, western blot results showed increased p53 and cytochrome *c* expression and suppression of topoisomerase IIα (Topo-IIα). Ab initio quantum mechanics (QM) predicted its electronic structure and molecular docking with DNA-Topo-II complex indicated that, with a unique binding, 8K-C3-D-SiQ could wrap around the DNA G-segment with two 1-methylquinolinium-8-oxypropyl substituents occupying both DNA cleavage sites. In conclusion, 8K-C3-D-SiQ may be considered a promising candidate for PDT due to its high singlet oxygen production, potent phototoxicity, topoisomerase inhibition, and apoptosis induction.

## 1. Introduction

Cancer is a disease characterized by cells that have lost their control mechanisms and continue to multiply uncontrollably [1]. In 2022, approximately 20 million people were diagnosed with cancer, and 10 million people lost their lives due to the disease [2]. Cancer also incurs high economic costs globally, which are expected to reach $25.2 trillion between 2020 and 2050 [3]. Endometrial cancer (EC) originates in the endometrial cells that form the inner lining of the uterus, and risk factors include genetic factors, aging, obesity, and increased estrogen levels [4]. Tumor suppressor gene loss, oncogene activation, and epigenetic changes play key roles in EC development [5]. In 2020, more than 417,000 new cases of EC and approximately 97,000 deaths were reported worldwide [6,7]. The primary approach in adjuvant therapy is

* Corresponding author.
*E-mail address:* burakbarut@ktu.edu.tr (B. Barut).

https://doi.org/10.1016/j.inoche.2026.116860
Received 21 March 2026; Received in revised form 3 May 2026; Accepted 16 May 2026
Available online 17 May 2026

surgery; chemotherapy and radiotherapy may be used as adjuncts. Although chemotherapy has reduced recurrence and improved survival in some subgroups, it has been insufficient in advanced stages [8].

Photodynamic therapy (PDT) is a targeted approach with high tumor selectivity and minimal side effects. In PDT, a photosensitizer, light, and molecular oxygen generate reactive oxygen species (ROS), which lead to cell death via apoptosis, necrosis, or autophagy [9–11]. Apoptosis is programmed cell death that occurs via intrinsic (mitochondrial) and extrinsic (death receptor) pathways; the p53 protein responds to DNA damage and regulates cell death [12,13]. In PDT, ideal photosensitizers must selectively accumulate in cancer tissue, exhibit low toxicity, absorb light in the 600–800 nm range, and be easily eliminated from the body [14,15]. Phthalocyanines are second-generation photosensitizers; they provide high light absorption, low toxicity in the dark, and favorable photochemical properties with metal ions [10,16]. Silicon (IV) phthalocyanines are ideal candidates due to their axial coordination sites. This hexacoordinated geometry allows for the attachment of two bulky substituents, which is thought to effectively prevent π–π stacking interactions. By reducing aggregation, the axial groups may significantly enhance singlet oxygen yields. In addition, while peripheral and non-peripheral substitution improve solubility and biocompatibility, the axial scaffold provides a versatile platform for bioactive ligands to target specific intracellular components [17,18].

Topoisomerases play a critical role in DNA replication and transcription; their overexpression in cancer cells contributes to uncontrolled proliferation [19]. Increased expression of topoisomerase IIα has been demonstrated in EC [20,21]. Topoisomerase inhibitors may enhance the efficacy of chemotherapy and PDT, but clinical drugs have serious side effects [22,23]. The integration of PDT and Topo-IIα inhibition may represent a promising dual-therapeutic strategy. While PDT-induced ROS can generate oxidative DNA lesions, the concurrent inhibition of Topo-IIα may hinder the repair of these damages and potentially stall the replication fork, which could contribute to a synergistic increase in genomic instability.

Quinoline is a nitrogen-containing heterocyclic aromatic compound found in the structure of many natural compounds. Quinoline and its derivatives have been reported in the literature to exhibit various biological and pharmacological activities, including antimalarial, antibacterial, antifungal, antihelminthic, cardiotonic, anticonvulsant, anti-inflammatory, and analgesic effects [24]. The main reason for selecting quinoline ligands in this study is that the potential of quinoline and its derivatives to inhibit topoisomerase enzymes has been reported in the literature [25–27]. Moreover, it has been shown that organic compounds containing quinoline have the capacity to generate singlet oxygen and can be used in PDT applications [28–30]. Additionally, the ability to quaternize the quinoline group via nitrogen atoms to render it water-soluble enhances the biocompatibility and biodistribution of these compounds in PDT, providing a significant advantage in their selection.

Based on this information, this study aims to investigate the PDT activities of newly synthesized quinoline-derived silicon phthalocyanine (8K-C3-D-Si and 8K-C3-D-SiQ) in a human endometrial cancer cell line (HEC-1B) and their potential effects on topoisomerases, which play a critical role in the pathophysiology of EC. The HEC-1B cell line was specifically selected for this study as it represents a model of moderately to poorly differentiated Type II endometrial carcinoma, which is typically more aggressive, less responsive to conventional hormone therapy, and often associated with p53 mutations and high Topo-IIα expression. Within this scope, the photochemical properties of the two synthesized compounds were first examined, followed by an evaluation of their PDT efficacy against HEC-1B cells. Subsequently, apoptosis/necrosis analysis was performed using flow cytometry to determine cell death mechanisms, and the expression of p53, cytochrome *c*, caspase-3, and Topo-IIα was examined using the western blot method to evaluate the suitability of the compounds for PDT.

## 2. Results and discussion

### 2.1. Synthesis and characterization

The synthetic route of the original compounds investigated in this study is illustrated schematically in Fig. 1. The structural features of the obtained compounds were characterized using FT-IR, $^{1}$H NMR, $^{13}$C NMR, UV–Vis, and mass spectrometric techniques. Initially, the compound coded as **8K-C3-Cl**, which is not original, was prepared following a previously reported procedure in the literature [31]. Subsequently, 8K-C3-Cl was dissolved in acetone, and 3,5-dihydroxybenzyl alcohol was added in the presence of potassium carbonate ($K_2CO_3$) and 18-crown-6. The reaction mixture was stirred at 70 °C for 48 h, during which the formation of **8K-C3-D-OH** was observed. In the $^{1}$H NMR spectrum of 8K-C3-D-OH recorded in DMSO-$d_6$, signals corresponding to 15 aromatic protons were observed in the range of 8.83–6.40 ppm, while a signal at 5.05 ppm was attributed to the Ar–$CH_2$–OH proton. Additionally, signals corresponding to 14 aliphatic protons appeared between 4.39 and 2.26 ppm (Fig. S1a). The $^{13}$C NMR spectrum exhibited resonances assigned to 13 aromatic carbons in the range of 160.00–99.93 ppm and 4 aliphatic carbons between 65.38 and 29.18 ppm (Fig. S1b). In the mass spectrum, a molecular ion peak at *m/z* 533.29 $[M + Na]^+$ (Fig. S2) was detected, which is consistent with the proposed molecular composition. The stretching vibrations of the functional groups belonging to 8K-C3-D-OH are presented in Fig. S3. In the subsequent step, 8K-C3-D-OH was reacted with silicon phthalocyanine dichloride ($SiPcCl_2$) in toluene in the presence of an appropriate amount of sodium hydride (NaH) at 110 °C for 24 h, leading to the formation of the axially disubstituted silicon phthalocyanine derivative **8K-C3-D-Si**. The FT-IR spectrum of 8K-C3-D-Si displayed characteristic aromatic C—H stretching vibrations at 3050–3003 $cm^{-1}$ and aliphatic C—H stretching vibrations at 2925–2861 $cm^{-1}$, while the absence of the O—H stretching band previously observed at approximately 3255 $cm^{-1}$ for 8K-C3-D-OH indicates the involvement of the hydroxyl group in axial coordination (Fig. S4). The $^{1}$H NMR spectrum of 8K-C3-D-Si recorded in $CDCl_3$ showed signals at 9.55–9.53 ppm and 8.24–8.21 ppm, corresponding to Pc–$H_\alpha$ and Pc–$H_\beta$ protons, respectively (Fig. 2a). Additional aromatic proton signals were observed at 8.96 ppm and within the range of 8.10–5.54 ppm, while aliphatic protons appeared between 4.14 and 2.07 ppm. Notably, a signal at −0.74 ppm was assigned to the Si–O–$CH_2$ protons. The $^{13}$C NMR spectrum revealed multiple carbon resonances distributed between 158.25 and 28.79 ppm (Fig. 2b). The UV–Vis spectrum of 8K-C3-D-Si recorded in chloroform exhibited characteristic Q and B bands at 678 and 351 nm, respectively, which are typical of silicon phthalocyanine systems (Fig. S5). In addition, the MALDI-TOF mass spectrum showed a molecular ion peak at *m/z* 1559.080 $[M]^+$ (Fig. 3a). In the final step, 8K-C3-D-Si was dissolved in chloroform and treated with an excess amount of methyl iodide ($CH_3I$) under dark conditions at room temperature for four days, resulting in the formation of the water-soluble silicon phthalocyanine derivative **8K-C3-D-SiQ**. The FT-IR spectrum of 8K-C3-D-SiQ (Fig. S6) was found to be largely similar to that of the precursor compound, displaying aromatic and aliphatic C—H stretching vibrations at 3035 $cm^{-1}$ and 2964–2873 $cm^{-1}$, respectively. The UV–Vis spectrum recorded in DMF showed Q and B bands at 676 and 348 nm, respectively (Fig. S5). The mass spectrum of 8K-C3-D-SiQ exhibited a prominent peak at *m/z* 556.413, which was tentatively assigned to the triply charged sodium adduct $[M - 3I + 3Na - 4H]^{3+}$ (Fig. 3b). This assignment may indicate that the detected ion originates from a partially quaternized/deiodinated species, since not all four nitrogen atoms are necessarily quaternized or retained with iodide counterions under MALDI conditions. Taken together, the spectroscopic and analytical data confirm that the synthesized silicon phthalocyanine derivatives are consistent with the proposed molecular structures. The obtained compounds were stored in a vacuum desiccator for use in subsequent studies.

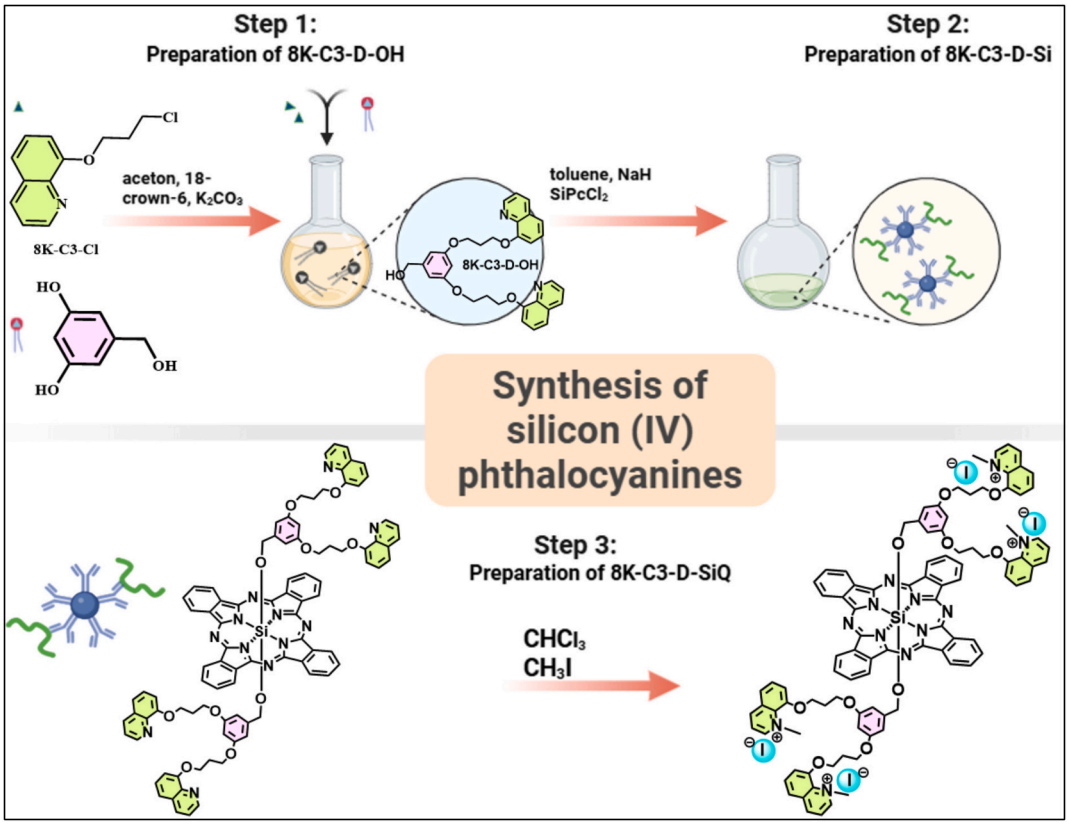


**Fig. 1.** The synthetic route of diaxially disubstituted quinoline silicon (IV) phthalocyanine (8K-C3-D-Si and 8K-C3-D-SiQ).

### 2.2. Photochemical properties of 8K-C3-D-Si and 8K-C3-D-SiQ

The PDT efficiency of photosensitizers is generally reduced due to the tendency of these compounds to aggregate, which adversely affects light absorption and the generation of cytotoxic singlet oxygen. To address this limitation, non-aggregating phthalocyanine derivatives have attracted considerable attention. In particular, silicon phthalocyanines bearing bulky axially coordinated substituents are known to exhibit negligible aggregation. These structural features make them promising candidates for high-performance PDT applications [17,32]. In accordance with the aggregation-related considerations discussed above, the aggregation tendencies of the two synthesized quinoline-substituted phthalocyanines were investigated. For this end, UV–Vis spectroscopic analyses were performed at varying concentrations (1–10 μM) in DMSO. As shown by the spectral profiles in Fig. 4, no significant aggregation behavior was observed for either compound within the studied concentration range.

#### 2.2.1. Singlet oxygen quantum yield ($\Phi_\Delta$) of 8K-C3-D-Si and 8K-C3-D-SiQ

PDT involves the light activation of photosensitizer compounds to generate ROS in cancer cells. The efficiency of this process depends on photostability and the capacity to produce singlet oxygen. High photostability ensures that the compound remains stable upon after photoactivation, while high singlet oxygen generation enables maximal biological efficacy in target cells [32,33]. In this study, singlet oxygen generation ability of the synthesized photosensitizers were evaluated in DMSO using 1,3-diphenylisobenzofuran (DPBF) as a singlet oxygen scavenger. All experiments were performed in triplicate and monitored using UV–Vis spectrophotometry. Singlet oxygen quantum yields were calculated based on the time-dependent decrease of DPBF. The singlet oxygen quantum yields of the synthesized compounds were determined as $\Phi_\Delta = 0.088 \pm 0.009$ for 8K-C3-D-Si and $\Phi_\Delta = 0.345 \pm 0.034$ for 8K-C3-D-SiQ. The water-soluble derivative (8K-C3-D-SiQ) exhibited higher singlet oxygen production (Fig. 5). In a study by Ünlü et al., the singlet oxygen quantum yield of the bis-{4-[(*E*)-(quinolin-3-ylimino)methyl] phenol} derivative silicon phthalocyanine compound was calculated to be 0.35 [34]. This value is similar to that of the quaternary (3,5-bis(3-(quinolin-8-yloxy)propoxy)phenyl) derivative of silicon phthalocyanine compound used in our study. However, in a study by Değirmencioğlu et al., the singlet oxygen quantum yields of silicon phthalocyanine compounds disubstituted with 1-(4-(3-(6-hydroxyhexyl)-3,4-dihydro-2H-benzo[e][1,3]oxazin-6-yl)piperazin-1-yl)ethanone and 1-(4-(3-(2-(2-hydroxyethoxy) ethyl)-3,4-dihydro-2H-benzo[e][1,3]oxazin-6-yl) piperazin-1-yl)ethanone, as well as their water-soluble derivatives were investigated. The singlet oxygen quantum yields for these compounds were reported as 0.04, 0.05, 0.41, and 0.31, respectively [35]. These results are consistent with our findings for the quaternized derivative, indicating a similar trend in which water-soluble or quaternized substituents enhance singlet oxygen generation.

#### 2.2.2. Photodegradation quantum yield ($\Phi_d$) of 8K-C3-D-Si and 8K-C3-D-SiQ

In this study, the resistance of the compounds to photodegradation was evaluated by exposing them to intense irradiation for 3000 s. All experiments were conducted in DMSO, and changes in absorbance were monitored as a function of time. As shown by the UV–Vis spectra (Fig. 6), all compounds exhibited photostability comparable to that of structurally related phthalocyanines reported in the literature. After irradiation, the Q-band absorbance of 8K-C3-D-SiQ decreased by about 25%. The calculated photodegradation quantum yields ($\Phi_d = 1.77 \times 10^{-5}$ for 8K-C3-D-Si, and $\Phi_d = 1.19 \times 10^{-5}$ for 8K-C3-D-SiQ) confirmed the good photostability of the compounds and their consistency with the values reported in the literature [36–38].

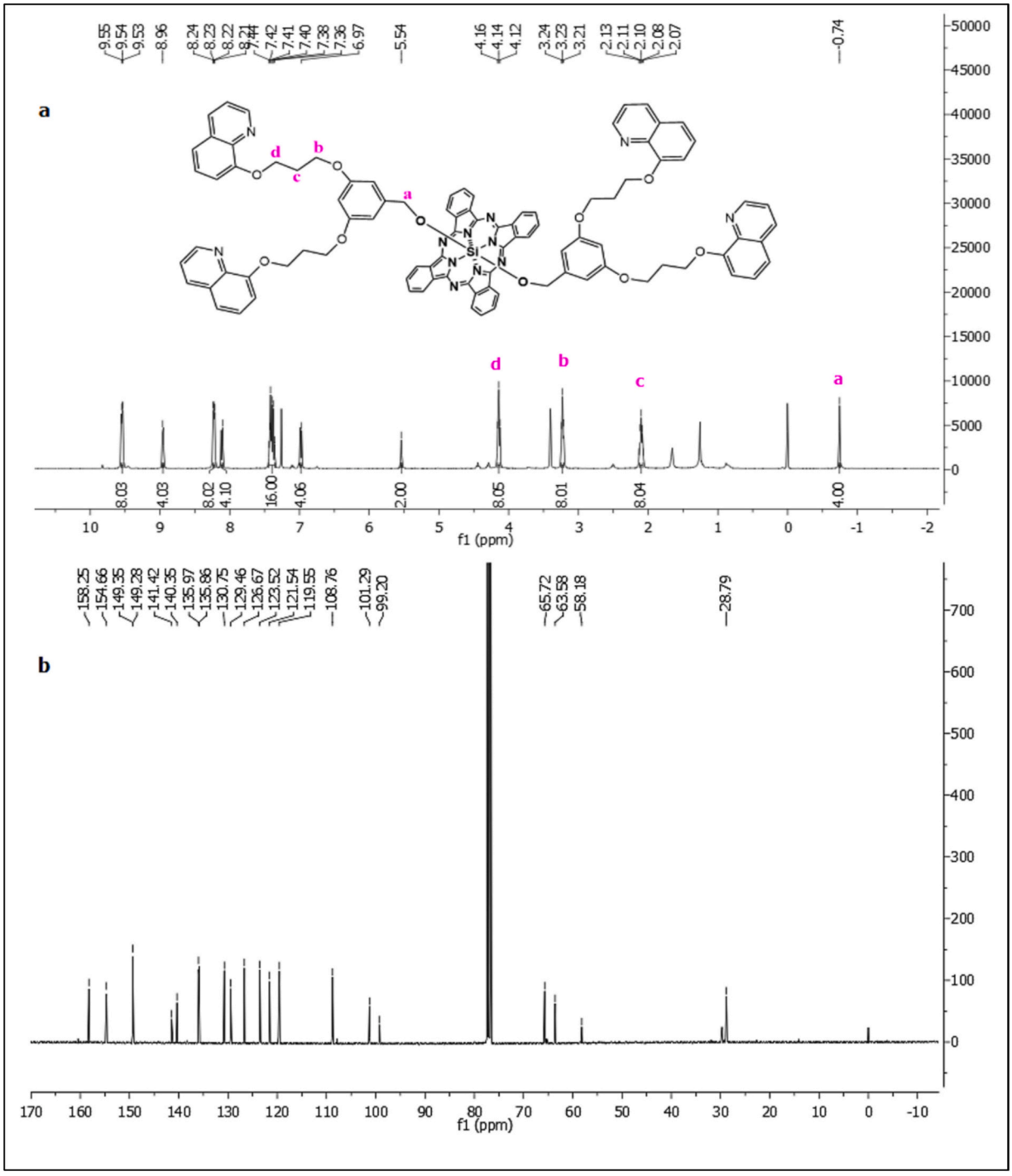


**Fig. 2.** a) $^{1}H$ and b) $^{13}C$ NMR spectra of 8K-C3-D-Si recorded in $CDCl_3$.

### 2.3. *In vitro PDT effects of 8K-C3-D-Si and 8K-C3-D-SiQ*

Following the photochemical analyses, the cytotoxic and phototoxic effects of 8K-C3-D-SiQ, which was considered more suitable for PDT, were evaluated. The effects of different concentrations (0.0003–1 μM) on cell viability were assessed under both dark and light conditions (660 nm, 4.5 mW/cm$^2$, 10 min) at incubation times of 24, 48, and 72 h. The results are presented in Table S1 and Fig. 7. Under dark conditions, cell viability generally remained at 80–100% at low concentrations (0.0003–0.01 μM), suggesting no significant cytotoxicity. On the other hand, at 0.03 μM, cell viability decreased to 58.8 ± 5.4% at 72 h, and at 0.1 μM, it decreased to 50.3 ± 7.9% under light irradiation. At 1 μM, cell viability under dark conditions remained between 53 and 78%, indicating limited dark toxicity. In contrast, a pronounced phototoxic effect was observed under light irradiation, with cell viability decreasing to 2.8 ± 0.5%, 1.6 ± 0.3%, and 2.3 ± 0.3% at 24, 48, and 72 h, respectively. Overall, 8K-C3-D-SiQ exhibited a strong phototoxic effect in the presence of light, particularly at concentrations of 0.03 μM and above, where cell viability was significantly reduced. At 1 μM, cell viability was almost completely abolished under light conditions. In contrast, toxicity under dark conditions remained limited, and cell viability was largely preserved.

The cytotoxic and phototoxic effects of 8K-C3-D-SiQ on L929 cells were investigated at different concentrations (0.0003–1 μM) and

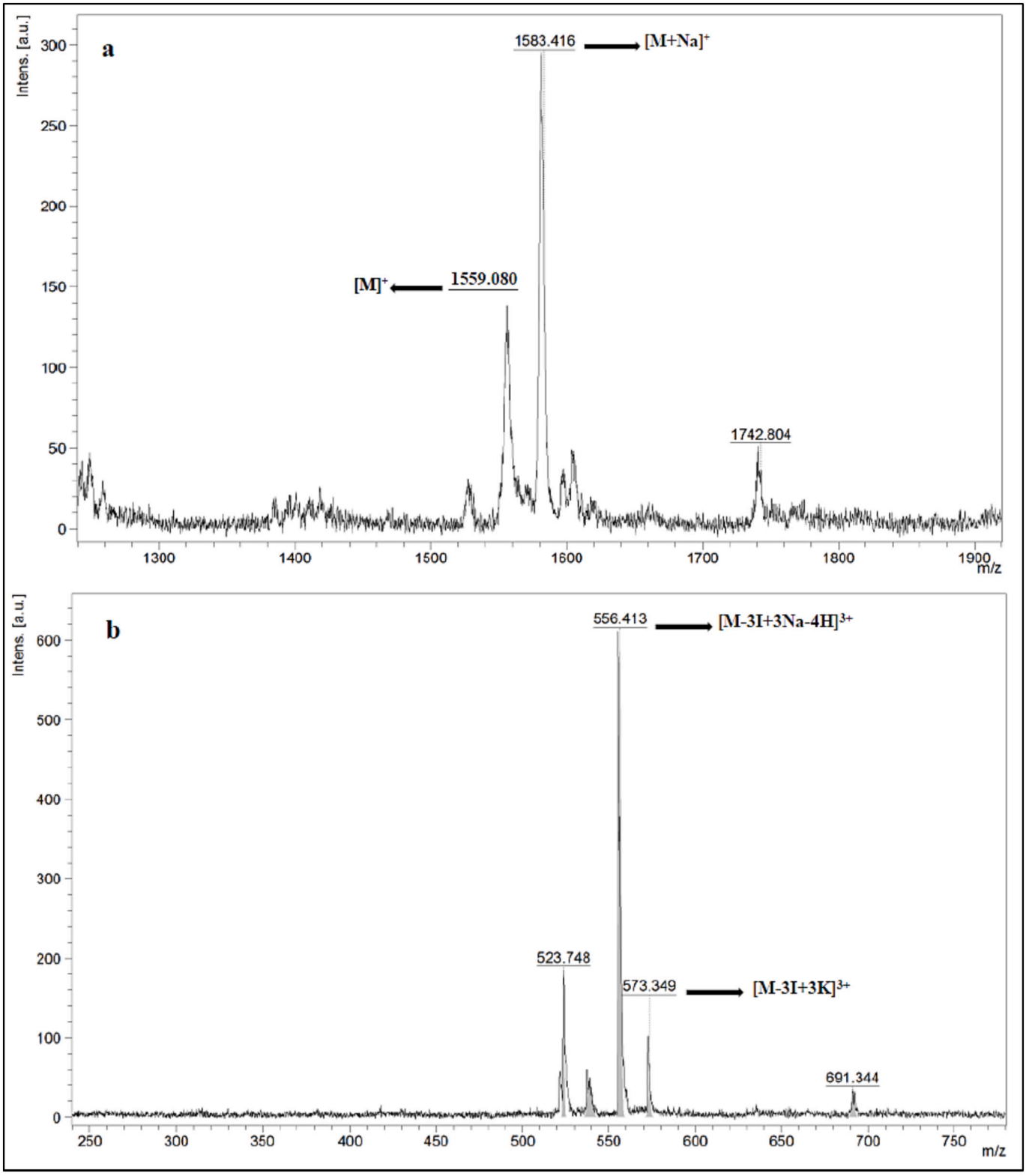


**Fig. 3.** MALDI-TOF mass spectra of the a) 8K-C3-D-Si and b) 8K-C3-D-SiQ.

incubation times (24, 48, and 72 h) (Table S2). At low concentrations (0.0003–0.003 μM), cell viability under dark conditions remained between 95 and 115%, while under light irradiation cell viability was largely preserved (82–103%), indicating no significant cytotoxicity. These findings suggest that the compound is relatively safe at low doses. In contrast, with increasing concentration, light-dependent toxicity became more pronounced. At concentrations of 0.01–0.03 μM, cell viability under light conditions decreased to 69 and 56%, respectively, whereas at 0.1 μM, cell viability further declined, reaching 23% at 72 h. At the highest concentration tested (1 μM), cell viability under light irradiation dropped to 4–8% at all time points, demonstrating a strong phototoxic effect of the compound.

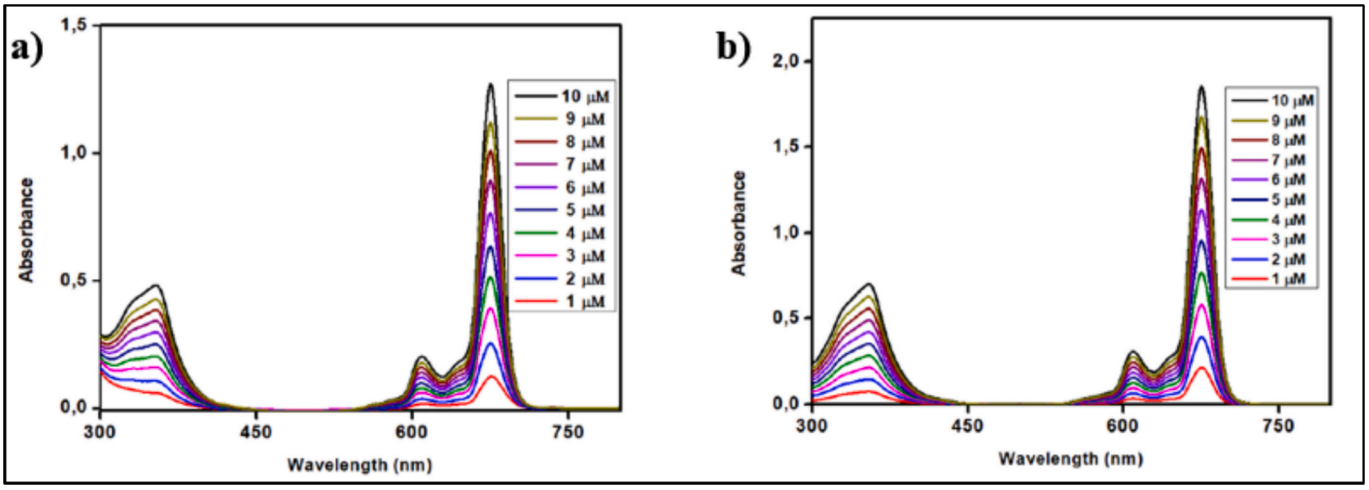


**Fig. 4.** Aggregation behavior of 8K-C3-D-Si and 8K-C3-D-SiQ compounds in DMSO. a) UV–Vis spectrum of 8K-C3-D-Si in DMSO; b) UV–Vis spectrum of 8K-C3-D-SiQ in DMSO.

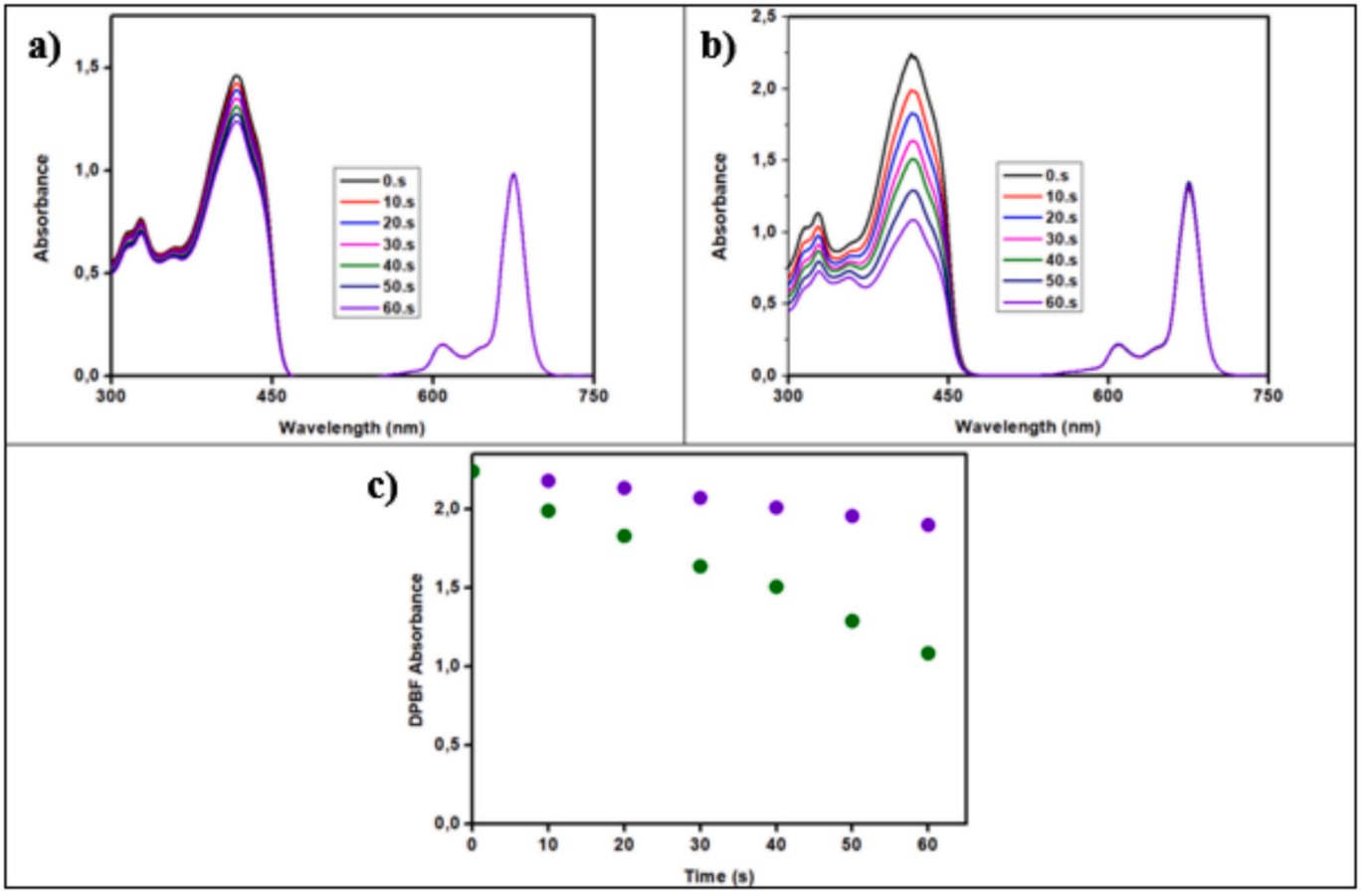


**Fig. 5.** Photochemical measurements of 8K-C3-D-Si and 8K-C3-D-SiQ. a) Change in DPBF concentration upon irradiation in the presence of 8K-C3-D-Si; b) Change in DPBF concentration upon irradiation in the presence of 8K-C3-D-SiQ; c) Time-dependent change in DPBF absorbance in the UV–Vis spectra of the compounds.

Although various studies have been conducted on EC cell lines in the presence of PDT agents such as hematoporphyrin and hypericin [39,40], the use of phthalocyanines against endometrial cancer cell lines is quite limited. One such study in this area involves a quaternized {3,5-bis[(3,5-bis{3-[3-(diethylamino)phenoxy]propoxy}benzyl)oxy]phenyl} derivative silicon phthalocyanine compound developed by our research group [41]. This compound exhibited effective phototoxic activity under white light (17.5 mW/cm$^2$, 60 min), but cell viability remained at approximately 20% at a concentration of 1 μM. In contrast, cell viability was almost eliminated at a concentration of 1 μM in the presence of quinoline-derived compounds. Chen et al. reported that quinoline-8-yloxy-substituted zinc phthalocyanine (ZnPc-Q1) exhibited strong photodynamic activity across multiple cancer cell lines (H460, Bel7402, HepG2, MDA-MB-231, KB, ACHN, and SH-SY5Y). Under light irradiation, the compound significantly reduced cell viability through antiproliferative and apoptotic effects, showing higher in vitro anticancer

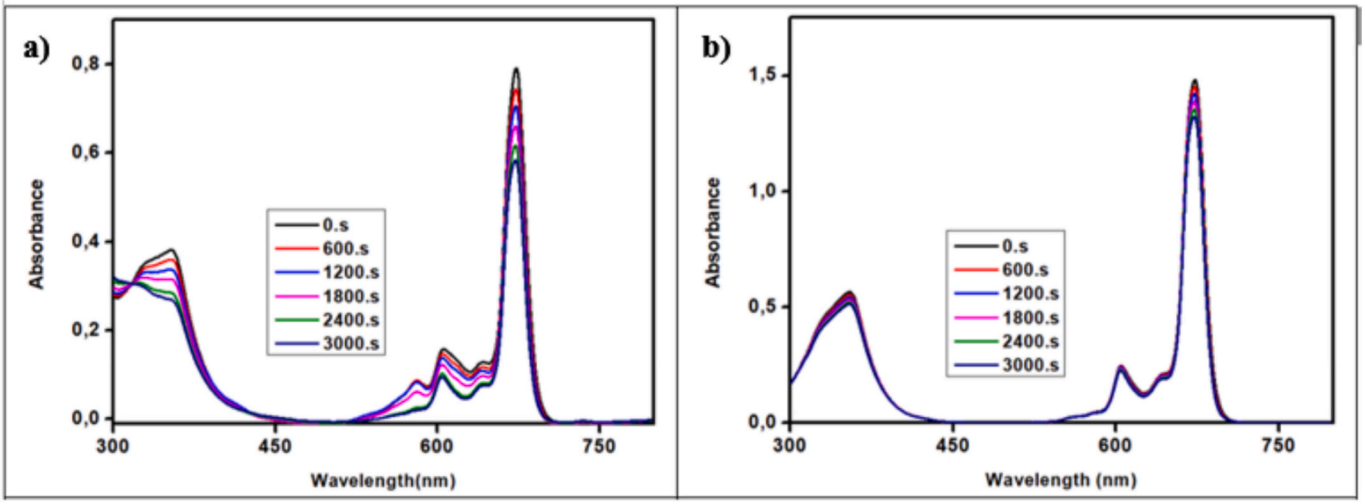


**Fig. 6.** Photostability of a) 8K-C3-D-Si and b) 8K-C3-D-SiQ.

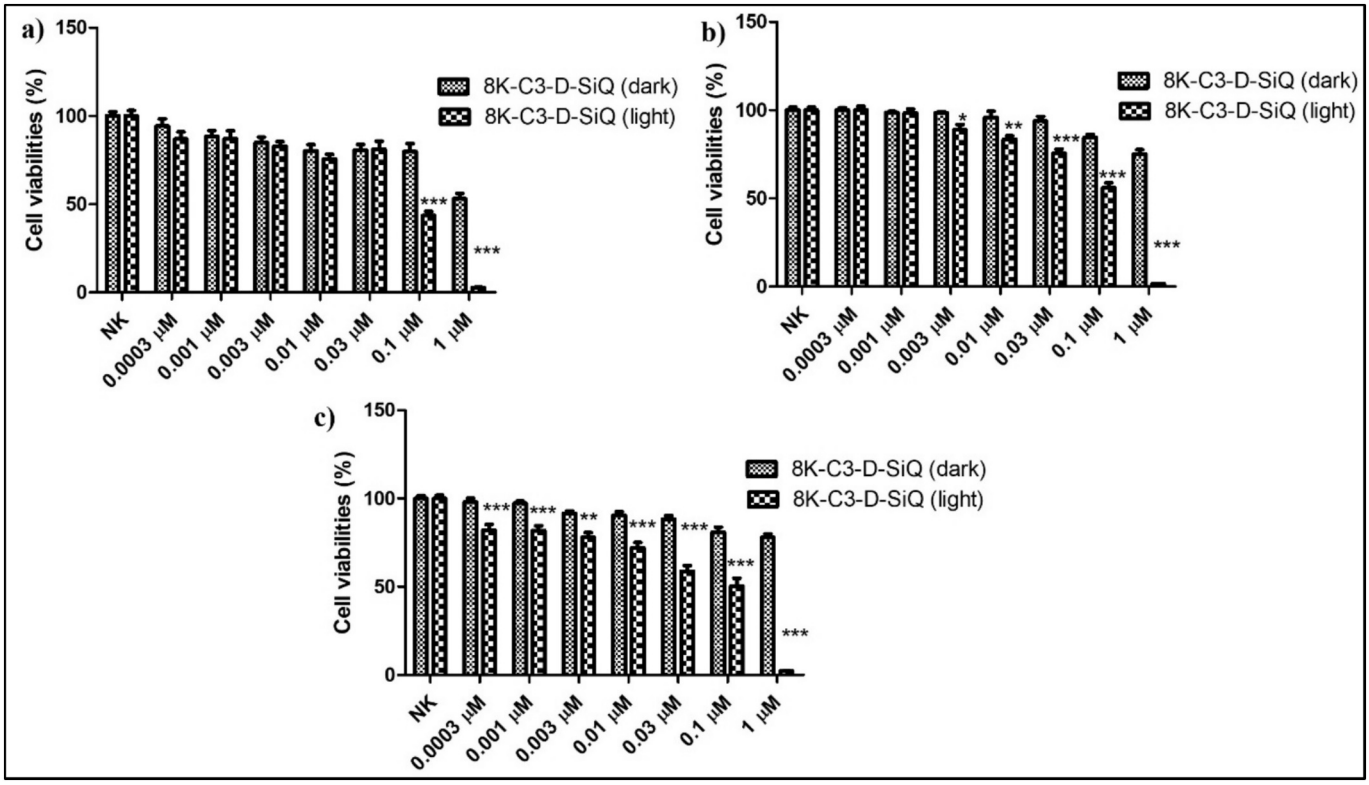


**Fig. 7.** Cytotoxic and phototoxic effects of 8K-C3-D-SiQ on HEC-1B cells. a) 24 h, b) 48 h, and c) 72 h incubation. Light irradiation (660 nm, 4.5 mW/cm$^2$) for 10 min. Statistical significance is indicated as $*p < 0.05$, $**p < 0.01$, and $***p < 0.001$ compared with the corresponding dark condition at the same concentration. Positive control: methylene blue (1 μM). Cell viability values for methylene blue were as follows: at 24 h, 61.40 ± 5.50% (dark) and 18.20 ± 3.70% (light); at 48 h, 41.10 ± 4.40% (dark) and 5.00 ± 0.90% (light); and at 72 h, 16.90 ± 3.30% (dark) and 4.20 ± 0.20% (light). (For interpretation of the references to colour in this figure legend, the reader is referred to the web version of this article.)

activity compared to Photofrin [42]. These findings indicate that the quinoline-derived compound has a stronger photodynamic potential in terms of PDT.

### 2.4. Effects of 8K-C3-D-SiQ on cell death mechanisms

#### 2.4.1. Apoptosis/necrosis analysis

In this study, flow cytometry was used to investigate the effects of 8K-C3-D-SiQ, which exhibited phototoxic activity in the HEC-1B cell line, on cell death mechanisms under light irradiation. The compound was evaluated at concentrations of 0.003, 0.01, 0.03, and 0.1 μM. The results are presented in Table S3 and Fig. 8. As shown in Table S3 and Fig. 8, 84.45 ± 1.79% of cells in the control group remained viable, indicating that the majority of cells maintained viability under normal conditions. At concentrations of 0.003 and 0.01 μM, cell viability remained high at 84.90 ± 0.63% and 80.81 ± 4.58%, respectively. In these groups, early apoptosis ranged between 2.2 and 2.3%, while late apoptosis showed a slight increase compared to the control group,

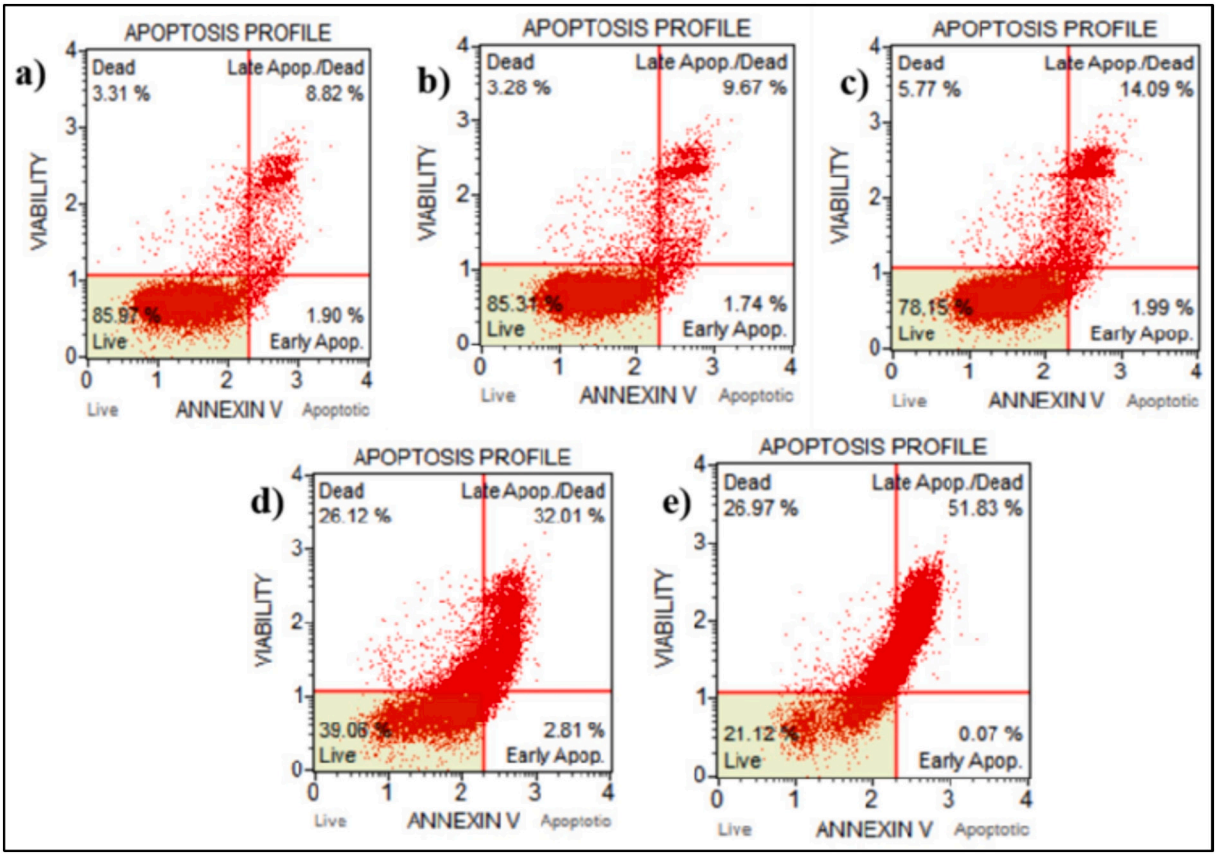


**Fig. 8.** Apoptosis/necrosis analysis of 8K-C3-D-SiQ under light irradiation on HEC-1B cells. a) negative control; b) 0.003 μM; c) 0.01 μM; d) 0.03 μM; e) 0.01 μM of 8K-C3-D-SiQ. Light irradiation (660 nm, 4.5 mW/cm$^2$) for 10 min.

reaching up to 12.45 ± 2.29%. No significant changes in necrosis rates were observed at these low concentrations. At 0.03 μM, cell viability decreased markedly to 44.53 ± 7.73%, indicating that more than half of the cells had entered cell death pathways. In this group, the late apoptosis rate increased to 24.98 ± 6.60%, while necrosis increased to 17.71 ± 12.13%. Additionally, early apoptosis was elevated to 3.04 ± 0.42% compared with the lower concentration groups. These findings suggest that both apoptotic and necrotic mechanisms were simultaneously activated at this concentration. At the highest concentration tested (0.1 μM), the most pronounced cytotoxic effect was observed. Cell viability declined to 22.94 ± 2.57%, with 54.03 ± 3.10% of cells undergoing late apoptosis and 22.74 ± 5.98% progressing to necrosis. The high rate of late apoptosis at 0.1 μM suggests a rapid activation of the cell death cascade. This fast progression likely stems from the dual action of 8K-C3-D-SiQ. The combined effect of PDT-induced oxidative stress and Topo-IIα inhibition creates a robust assault on the cell. Such an intense multi-level impact may contribute to the progression toward late-stage apoptosis, potentially reducing the involvement of early apoptotic events. Early apoptosis levels remained low, indicating that most cells directly advanced to late apoptosis or necrosis. These results show that 8K-C3-D-SiQ induces cell death in a dose-dependent manner under light irradiation; cell viability is preserved at low doses, whereas late apoptosis appears to predominate.

### 2.4.2. *Western blot analysis*

In this study, the effects of 8K-C3-D-SiQ on cell death mechanisms in the HEC-1B cell line were investigated by analyzing the expression levels of p53, cytochrome *c*, and caspase-3 (widely accepted markers of apoptotic pathways) using western blotting. In addition, the expression levels of Topo-IIα proteins, which plays and important role in cancer pathophysiology, were also analyzed by western blotting. The results are presented in Fig. 9. Under light irradiation, Topo-IIα expression was significantly decreased in the 8K-C3-D-SiQ-treated group compared to the control group (***$p < 0.001$). In the methylene blue group, Topo-IIα expression was almost completely suppressed. No significant change in caspase-3 expression was observed in the 8K-C3-D-SiQ-treated group compared to the control, whereas caspase-3 expression was not detectable in the methylene blue group. The expression of p53, a key protein involved in apoptosis and the DNA damage response, was significantly upregulated in the 8K-C3-D-SiQ-treated cells (***$p < 0.001$), whereas no expression was detected in the methylene blue group. Similarly, the levels of cytochrome *c*, a marker of mitochondrial apoptosis, were significantly increased in the 8K-C3-D-SiQ treated group compared to the control (*$p < 0.05$), while no expression was observed in the methylene blue group.

The obtained findings indicate that the 8K-C3-D-SiQ exerts a multifaceted effect by both suppressing cell proliferation and activating apoptotic mechanisms. First, the significant decrease in Topo-IIα expression suggests that 8K-C3-D-SiQ exerts a regulatory effect on DNA topoisomerase enzymes. Inhibition of Topo-IIα may disrupt DNA replication and chromosome segregation, thereby suppressing cell cycle progression [43]. The observed increase in p53 protein expression indicates that the compound activates the DNA damage response and stimulates tumor suppressor mechanisms within the cells. Activation of p53 is known to induce both cell cycle arrest and apoptosis [44]. The increased release of cytochrome *c* into the cytoplasm further indicates activation of the mitochondrial apoptotic pathway [45]. The upregulation of p53 and cytochrome *c* strongly supports that 8K-C3-D-SiQ induces mitochondria-mediated apoptosis. However, the lack of significant caspase-3 change suggests a potential shift toward a caspase-independent mitochondrial pathway. In such cases, factors like AIF or Endo G can drive programmed death even without executioner caspase

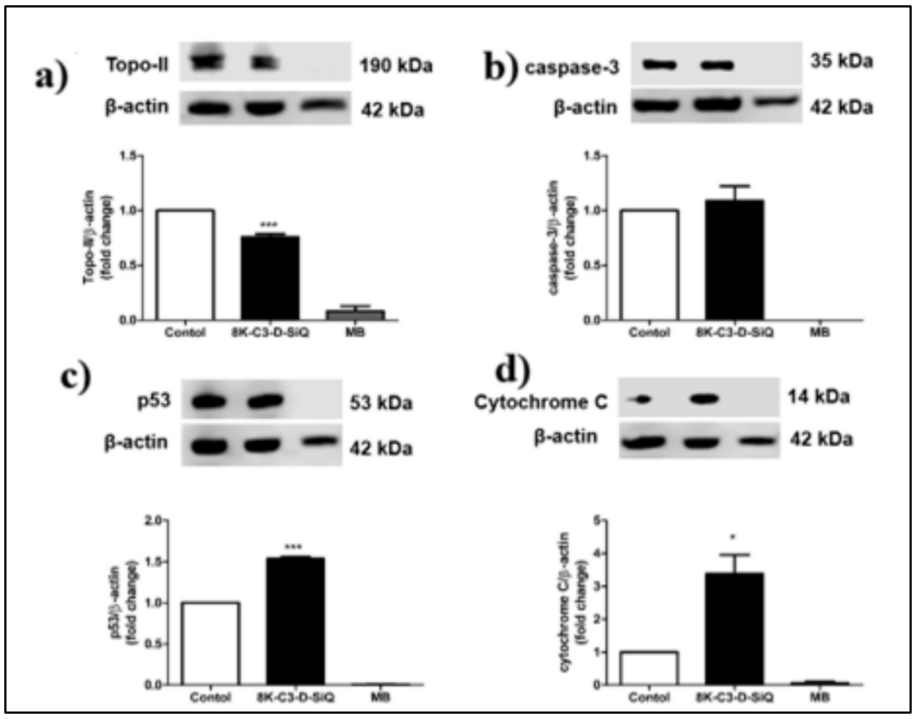


**Fig. 9.** Expression of Topo II, caspase-3, p53, and cytochrome *c* on HEC-1B cells under light exposure in the presence of 8K-C3-D-SiQ. a) Densitometric analysis of Topo II; b) Densitometric analysis of caspase-3; c) Densitometric analysis of p53; d) Densitometric analysis of cytochrome *c* ($n = 3$). Light irradiation (660 nm, 4.5 mW/cm$^2$) for 10 min. *p < 0.05, **p < 0.01, ***p < 0.001 indicate a significant difference compared to the control group (Student's *t*-test).

activation [46]. Alternatively, this result may be due to a time-dependent caspase-3 peak that was not captured within the 24-h experimental window. Furthermore, while methylene blue is known for its excellent light-induced ROS yield, its application is often limited by a lack of targeting and rapid clearance in its free form [47]. In this study, the complete absence of protein bands in the methylene blue-treated group reflects this high ROS output, leading to non-specific cellular collapse and protein degradation. In contrast, the selective protein changes in the 8K-C3-D-SiQ group demonstrate a more regulated, targeted response. Overall, these findings suggest that, under light irradiation, 8K-C3-D-SiQ activates apoptotic mechanisms in HEC-1B cells through a combination of Topo-IIα inhibition and mitochondrial signaling.

### 2.5. Molecular modelling

#### 2.5.1. Molecular geometry of 8K-C3-D-Si and 8K-C3-D-SiQ

Molecular structures of the silicon complexes were predicted using DFT calculations, which suggested certain variations in their geometries. Regarding 8K-C3-D-Si, the axial groups connected to silicon were aligned quasi-parallel with respect to phthalocyanine ring. Fig. 10A illustrates the extensive array of intramolecular electrostatic contacts between the central phthalocyanine ring and 8K-C3-D-O-substituents, which were much more spread out in the case of 8K-C3-D-SiQ (Fig. 10d). Specifically, one 1-methylquinolinium-8-oxypropyl substituent attached to each 3,5-dihydroxybenzyl was axially stretched out, while the other 1-methylquinolinium-8-oxypropyl substituent stretched parallel to the phthalocyanine. This arrangement was clearly apparent in the optimized structure. Frontier molecular orbital (FMO) analysis also revealed notable differences between the complexes. While HOMO and LUMO orbitals were mainly localized around the phthalocyanine of 8K-C3-D-Si close to the silicon center (indicating a site vulnerable to chemical modifications), LUMO orbitals were predicted to be localized on one of the parallel 1-methylquinolinium rings of 8K-C3-D-SiQ, which we will hereafter be referred to as the "LUMO ring" (Fig. 10).

#### 2.5.2. Molecular docking with Topo-II

Topoisomerase poisons such as etoposide are known to target the DNA cleavage sites of the enzyme-DNA complex. Crystallographic studies have established that each etoposide molecule intercalates between the −1 and +1 DNA base pairs at the cleavage site via its tetracyclic central unit while the fourth ring fits into a pocket of DNA gate and the glycone moiety extends to enzyme-DNA interface [48,49]. Prior to docking of the silicon complexes, we tested the methodology by redocking etoposide to both DNA cleavage sites in order to evaluate the ability of the method to reproduce experimentally established binding modes. The predicted poses of etoposide were similar to its original orientations in the crystallographic structure in both cleavage sites as evidenced by the RMSD values (0.3603 and 0.3335 Å). For docking of the silicon complexes a large docking region covering both DNA cleavage sites was defined. However, the docking experiment produced poses only for 8K-C3-D-SiQ with docking score (−13.6 kcal/mol) slightly better than those of etoposide (−11.3 and −12.2 kcal/mol). The predicted binding pose of 8K-C3-D-SiQ revealed an interesting but effective interaction with the G-segment approaching from the minor groove with the help of the 1-methylquinolinium-8-oxypropyl substituents, which interacted with different parts of the double strand, like the arms of an octopus, including both cleavage sites (Fig. 11). One of these substituents intercalated at the same position as etoposide, stacking between thymine (+1) and cytosine (−1), and forming a hydrogen bond with Arg487, similar to etoposide, while the other stacked with adenine (−1) at the second cleavage site. The other two substituents, including the LUMO-ring, interacted with the phosphate backbone, while the central phthalocyanine ring was positioned in the minor groove (Fig. 11). This high-affinity binding mode of 8K-C3-D-SiQ may explain how effectively the compound stabilizes the DNA–Topo-II complex, thereby stalling the DNA repair process.

## 3. Conclusion

In this study, the potential of quinoline-substituted silicon

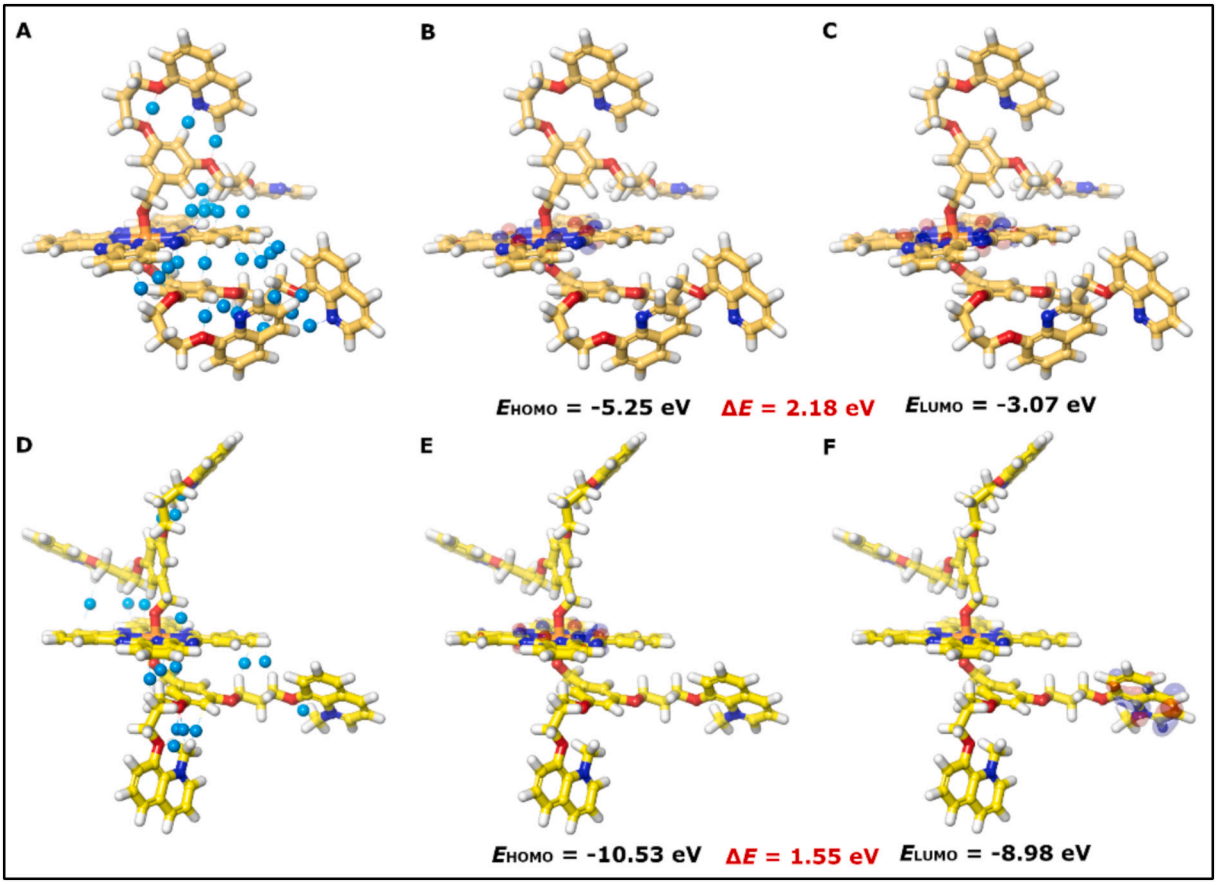


**Fig. 10.** Predicted 3D molecular structures, HOMO and LUMO orbitals of (A-C) 8K-C3-D-Si and (D—F) 8K-C3-D-SiQ, respectively. Ligands are shown in colour stick-and-ball representation, intramolecular electrostatic interactions as blue spheres, HOMO and LUMO orbitals as colour surfaces. (For interpretation of the references to colour in this figure legend, the reader is referred to the web version of this article.)

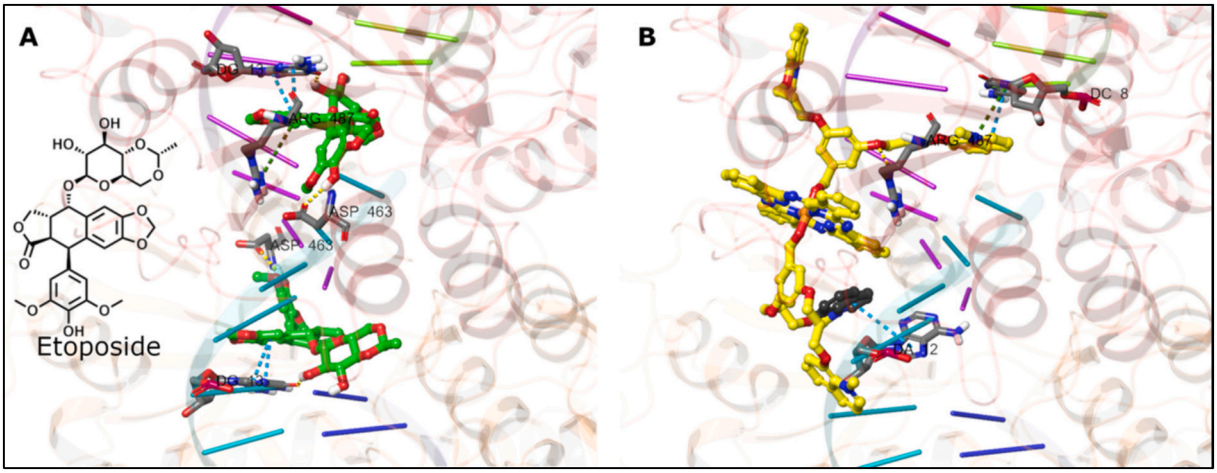


**Fig. 11.** Crystallographic binding of etoposide molecules in the DNA cleavage sites of DNA-Topo-II complex acrtive site (A) and the predicted binding of 8K-C3-D-SiQ in the same site (B). Ligands are shown in colour stick-and-ball representation, amino acids and DNA bases as grey sticks, protein and DNA backbones as colour cartoons, and electrostatic interactions as colour dashed-lines.

phthalocyanine derivatives (8K-C3-D-Si and 8K-C3-D-SiQ) for PDT was evaluated. UV–Vis spectroscopic analyses revealed that the synthesized compounds showed no significant aggregation, and this may represent a significant advantage in terms of PDT efficiency. Photochemical evaluations showed that 8K-C3-D-SiQ showed improved performance, particularly due to its high singlet oxygen production capacity and good photostability consistent with those reported in the literature. Cellular studies showed that the 8K-C3-D-SiQ exhibited low toxicity under dark conditions, but in the presence of light, it produced a strong phototoxic effect in a dose-dependent manner. Flow cytometry analyses revealed that cell viability was largely preserved at low concentrations, while cell death increased significantly with increasing concentrations, with late apoptosis becoming predominant, especially at high doses. Western blot analyses showed that the 8K-C3-D-SiQ activated mitochondrial

apoptotic pathways as indicated by increased p53 and cytochrome *c* expression under light irradiation, while also suggesting an inhibitory effect on cell proliferation by suppressing Topo-IIα expression. Molecular modelling predicted the 3D geometry of the silicon complexes, as well as how the structure of 8K-C3-D-SiQ could lead to a highly effective binding to and stabilization of DNA–Topo-II complex. When all these findings are considered together, 8K-C3-D-SiQ may represent a promising photosensitizer candidate for PDT applications due to its high photodynamic activity, favorable photochemical properties, and ability to induce apoptosis through mitochondria-mediated mechanisms.

## 4. Experimental section

### 4.1. Materials and methods

Details of the materials and equipment, photochemical studies, in vitro PDT experiments, apoptosis/necrosis detection assays, western blotting analysis, and in silico studies of Topo-IIα studies are provided in the Supplementary Information.

### 4.2. Synthesis

#### 4.2.1. Synthesis of (3,5-bis(3-(quinolin-8-yloxy)propoxy)phenyl)methanol (8K-C3-D-OH)

In a 250 mL round-bottom flask, 0.40 g (2.8 mmol) of 3,5-dihydroxybenzyl alcohol and 2.85 g (20.44 mmol) of anhydrous $K_2CO_3$ were dissolved in 50 mL of acetone. Subsequently, 1.3 g (5.9 mmol) of 8K-C3-Cl compound and 0.59 g (2.24 mmol) of 18-crown-6 were added to the reaction mixture, and the system was degassed under nitrogen. The reaction was stirred at 70 °C for 48 h under a nitrogen atmosphere. After completion, the reaction mixture was filtered through black band filter paper, and the solvent was removed by evaporation. The crude product was purified by column chromatography on neutral silica gel using chloroform as the eluent. The product was obtained in 0.90 g yield of 62%. IR (ATR, $\nu_{max}$/cm$^{-1}$): 3255 (O—H), 3066 (Ar—H), 2930–2826 (aliphatic C—H), 1597 (C=N), 1574, 1505 (C=C), 1456, 1377, 1321, 1262 (Ar–C–O), 1164, 1109, 1061, 1031, 1010, 971, 821, 790, 729, 680. $^1$H NMR (DMSO-$d_6$, $\delta$ ppm): 8.83 (d, 2H, Ar—H), 8.27 (d, 2H, Ar—H), 7.50 (t, 2H, Ar—H), 7.46 (d, 4H, Ar—H), 7.19 (t, 2H, Ar—H), 6.50 (s, 2H, Ar—H), 6.40 (s, 1H, Ar—H), 5.05 (t, 1H, –OH), 4.39 (s, 2H, CH₂–OH), 4.28 (t, 4H, CH₂–O–Ar), 4.17 (t, 4H, CH₂–O–Ar), 2.26 (m, 4H, –CH$_2$–). $^{13}$C NMR (DMSO-$d_6$, $\delta$ ppm): 160.00, 154.77, 149.40, 145.67, 140.17, 136.21, 129.47, 127.26, 122.25, 120.07, 109.87, 105.17, 99.93, 65.38, 64.70, 63.22, 29.18. MS (ESI), *m/z*: 533.29 [M+Na]$^+$.

#### 4.2.2. Synthesis of 8K-C3-D-Si

In a 50 mL single-neck round-bottom flask, 100 mg (0.16 mmol) of silicon phthalocyanine dichloride was dissolved in 10 mL of dry toluene. Subsequently, 166 mg (0.33 mmol) of (3,5-bis(3-(quinolin-8-yloxy) propoxy)phenyl)methanol (8K-C3-D-OH) was added to the reaction mixture, which was stirred for 10 min at room temperature under a nitrogen atmosphere. Then, 8 mg (0.33 mmol) of NaH was rapidly added, and the reaction mixture was degassed by purging with nitrogen gas. The reaction mixure was stirred at 110 °C for 24 h under a nitrogen atmosphere. After cooling to room temperature, the solvent was completely removed by evaporation. The crude product was purified by column chromatography on silica gel using a $CHCl_3$:$CH_3OH$ (60:1, *v*/v) solvent system as the eluent. The product was obtained as a solid (134 mg, 52% yield) with a decomposition temperature above 300 °C. IR (ATR, $\nu_{max}$/cm$^{-1}$): 3050–3003 (Ar—H), 2925–2861 (aliphatic C—H), 1597, 1569, 1499, 1464, 1427, 1376, 1334, 1317, 1289, 1252, 1166, 1102, 1077, 910, 867, 820, 790, 743. $^1$H NMR (400 MHz, $CDCl_3$, $\delta$ ppm): 9.55–9.53 (m, 8H, Pc–Hα), 8.96 (d, 4H, Ar—H), 8.24–8.21 (m, 8H, Pc–H), 8.10 (d, 4H, Ar—H), 7.44–7.36 (m, 16H, Ar—H), 6.97 (d, 4H, Ar—H), 5.54 (s, 2H, Ar—H), 4.14 (t, 8H, Ar–OCH₂)$_d$, 3.23 (t, 8H, Ar–OCH₂)$_b$, 2.13–2.07 (m, 8H, –CH₂–), −0.74 (s, 4H, Si–O–CH₂). $^{13}$C NMR (100 MHz, $CDCl_3$, $\delta$ ppm): 158.25, 154.66, 149.35, 149.28, 141.42, 140.35, 135.97, 135.86, 130.75, 129.46, 126.67, 123.52, 121.54, 119.55, 108.76, 101.29, 99.20, 65.72, 63.58, 58.18, 28.79. UV–Vis ($CHCl_3$) $\lambda_{max}$, nm (log ε): 678 (4.99), 647 (4.20), 608 (4.25), 351 (4.50). MALDI–TOF–MS *m/z*: 1559.080 [M]$^+$.

#### 4.2.3. Synthesis of 8K-C3-D-SiQ

In a 50 mL single-neck round-bottom flask, 25 mg (0.016 mmol) of the silicon phthalocyanine compound coded as 8K-C3-D-Si was dissolved in 2.0 mL of $CHCl_3$. Subsequently, 2.0 mL of iodomethane ($CH_3I$) was added to the reaction mixture, which was then stirred for 4 days in the dark at room temperature. At the end of the reaction period, the precipitated solid was filtered through a glass frit and washed successively with chloroform and diethyl ether to remove unreacted materials. The resulting product was stored in a vacuum desiccator for further use. The product was obtained as a solid (20 mg, 59% yield) with a decomposition temperature above 300 °C. IR (ATR, $\nu_{max}$/cm$^{-1}$): 3035 (Ar—H), 2964–2873 (aliphatic C—H), 1596, 1532, 1459, 1429, 1391, 1333, 1288, 1158, 1121, 1078, 910, 823, 738. UV–Vis (DMF) $\lambda_{max}$, nm (log ε): 676 (4.98), 642 (4.20), 611 (4.26), 348 (4.71). MALDI–TOF–MS *m/z*: 556.413 [M-3I + 3Na-4H]$^{3+}$.

## CRediT authorship contribution statement

**Gökçe Seyhan:** Writing – original draft, Methodology, Investigation, Data curation, Conceptualization. **Yasemin Altun Ali:** Methodology, Investigation, Data curation. **Elif Nur Barut:** Writing – original draft, Methodology, Investigation. **Manar M. Amin:** Writing – review & editing, Methodology, Investigation. **Turgut Keles:** Writing – original draft, Methodology. **Suat Sari:** Writing – review & editing, Writing – original draft, Methodology, Investigation. **Baybars Koksoy:** Writing – original draft, Methodology, Investigation. **Can Özgür Yalcin:** Methodology, Investigation, Conceptualization. **Zekeriya Biyiklioglu:** Writing – review & editing, Methodology, Conceptualization. **Burak Barut:** Writing – original draft, Supervision, Methodology, Investigation, Funding acquisition, Conceptualization.

## Declaration of competing interest

The authors declare that they have no known competing financial interests or personal relationships that could have appeared to influence the work reported in this paper.

## Acknowledgements

This work was supported by The Health Institutes of Türkiye (TUSEB) (Project number: 39060). Dr. Barut would like to thank the The Turkish Academy of Sciences (TÜBA-GEBİP) Outstanding Young Scientists Award Program for its support. OpenAI was utilized to enhance the wording used in the text.

## Appendix A. Supplementary data

Supplementary data to this article can be found online at https://doi.org/10.1016/j.inoche.2026.116860.

## Data availability

No data was used for the research described in the article.

## References

[1] J.S. Brown, S.R. Amend, R.H. Austin, R.A. Gatenby, E.U. Hammarlund, K.J. Pienta, Updating the definition of cancer, Mol. Cancer Res. 21 (11) (2023) 1142–1147.
[2] F. Bray, M. Laversanne, H. Sung, J. Ferlay, R.L. Siegel, I. Soerjomataram, A. Jemal, Global cancer statistics 2022: GLOBOCAN estimates of incidence and mortality

worldwide for 36 cancers in 185 countries, CA Cancer J. Clin. 74 (3) (2024) 229–263.
[3] S. Chen, Z. Cao, K. Prettner, M. Kuhn, J. Yang, L. Jiao, C. Wang, Estimates and projections of the global economic cost of 29 cancers in 204 countries and territories from 2020 to 2050, JAMA Oncol. 9 (4) (2023) 465–472.
[4] T. Dörk, P. Hillemanns, C. Tempfer, J. Breu, M.C. Fleisch, Genetic susceptibility to endometrial cancer: risk factors and clinical management, Cancers 12 (9) (2020) 2407.
[5] F. Inoue, K. Sone, Y. Toyohara, Y. Takahashi, A. Kukita, A. Hara, Y. Osuga, Targeting epigenetic regulators for endometrial cancer therapy: its molecular biology and potential clinical applications, Int. J. Mol. Sci. 22 (5) (2021) 2305.
[6] B.H.M. Hoseyni, H. Lanjanian, Y.Z. Beigi, M. Salimi, F. Zare-Mirakabad, A. Masoudi-Nejad, Molecular landscape of endometrioid cancer: integrating multiomics and deep learning for personalized survival prediction, Comput. Biol. Med. 192 (2025) 110284.
[7] World Cancer Research Fund International (WCRFI), Endometrial cancer statistics, 2026.
[8] E.D. Donnelly, D.E. Matei, E.M. Hinchcliff, E.J. Tanner, Treatment of endometrial cancer: updates and future directives, Adv. Oncol. 3 (1) (2023) 11–19.
[9] A. Żołyniak-Brzuchacz, E. Barnas, D. Bartusik-Aebisher, D. Aebisher, The use of photodynamic therapy in the treatment ofvendometrial cancer—a review of the literature, Int. J. Mol. Sci. 25 (16) (2024) 8772.
[10] G. Seyhan, B. Barut, T. Keleş, Z. Biyiklioğlu, In vitro/in vivo cancer studies of phthalocyanines in photodynamic therapy: a review, ChemistrySelect 10 (26) (2025) e01168.
[11] M. Li, Z. Tai, J. Liu, R. Wang, H. Yan, Q. Zhu, Z. Chen, Lysosome-targeted 5,15-diaryltetraacenaphthoporphyrin as a promising immunoinducer for enhanced photodynamic therapy in melanoma, Eur. J. Med. Chem. 304 (2026) 118472.
[12] Y. Abuetabh, H.H. Wu, C. Chai, H. Al Yousef, S. Persad, C.M. Sergi, R. Leng, DNA damage response revisited: the p53 family and its regulators provide endless cancer therapy opportunities, Exp. Mol. Med. 54 (10) (2022) 1658–1669.
[13] M. Mustafa, R. Ahmad, I.Q. Tantry, W. Ahmad, S. Siddiqui, M. Alam, K. Abbas, M. I. Hassan, S. Habib, S. Islam, Apoptosis: a comprehensive overview of signaling pathways, morphological changes, and physiological significance and therapeutic implications, Cells 13 (22) (2024) 1838.
[14] N.S. Kuzmina, E.A. Fedotova, P. Jankovic, G.P. Gribova, A.V. Nyuchev, A. Y. Fedorov, V.F. Otvagin, Enhancing precision in photodynamic therapy: innovations in light-driven and bioorthogonal activation, Pharmaceutics 16 (2024) 479.
[15] A.N. Al-Jamal, A.F. Al-Hussainy, B.A. Mohammed, H.H. Abbas, I.M. Kadhim, Z. H. Ward, D.K. Mahapatra, T.M. Joseph, E. Kianfari, S. Thomas, Photodynamic therapy (PDT) in drug delivery: nano-innovations enhancing treatment outcomes, Health Sci. Rev. 14 (2025) 100218.
[16] L.C. Nene, H. Abrahamse, Design consideration of phthalocyanines as sensitizers for enhanced sono-photodynamic combinatorial therapy of cancer, Acta Pharm. Sin. B 14 (3) (2024) 1077–1097.
[17] P. Sen, T. Nyokong, A novel axially palladium (II)-Schiff base complex substituted silicon (IV) phthalocyanine: synthesis, characterization, photophysicochemical properties and photodynamic antimicrobial chemotherapy activity against *Staphylococcus aureus*, Polyhedron 173 (2019) 114135.
[18] B. Barut, E.N. Barut, C.O. Yalçın, Y. Altun Ali, D. Akkaya, G. Seyhan, S. Engin, Z. Biyiklioglu, The synthesis and therapeutic effect of silicon(IV) phthalocyanines for colorectal cancer cells in photodynamic therapy by altering Wnt/β-catenin and apoptotic signaling, J. Photochem. Photobiol. A: Chem. 453 (2024) 115663.
[19] X. Deng, X. Yang, Q. Yu, Z. Xia, Y. Wang, R. Huang, H. Chen, W. Li, Y. He, Design, synthesis and biological evaluation of 3-arylisoquinoline derivatives as topoisomerase IIα inhibitors for the therapy of small cell lung cancer, Bioorg. Med. Chem. 129 (2025) 118299.
[20] V. Yilmaz, O.T. Yalçın, S.S. Ozalp, N. Tel, K. Bildirici, Prognostic significance of DNA topoisomerase II-α (Ki-S1) immunoexpression in endometrial carcinoma, Eur. J. Gynaecol. Oncol. 23 (6) (2002) 540–544.
[21] J.Y. Kim, S.G. Lee, J.Y. Chung, Y.J. Kim, J.E. Park, H. Koh, J.M. Kim, Ellipticine induces apoptosis in human endometrial cancer cells: the potential involvement of reactive oxygen species and mitogen-activated protein kinases, Toxicology 289 (2–3) (2011) 91–102.
[22] I. Postiglione, A. Chiaviello, G. Palumbo, Enhancing photodynamic therapy efficacy by combination therapy: dated, current and oncoming strategies, Cancers 3 (2) (2011) 2597–2629.
[23] R. Weijer, M. Broekgaarden, M. Krekorian, L.K. Alles, A.C. van Wijk, C. Mackaaij, M. Heger, Inhibition of hypoxia-inducible factor 1 and topoisomerase with acriflavine sensitizes perihilar cholangiocarcinomas to photodynamic therapy, Oncotarget 7 (3) (2016) 3341–3353.
[24] P. Yadav, K. Shah, Quinolines, a perpetual, multipurpose scaffold in medicinal chemistry, Bioorg. Chem. 109 (2021) 104639.
[25] K.G. Byler, C. Wang, W.N. Setzer, Quinoline alkaloids as intercalative topoisomerase inhibitors, J. Mol. Model. 15 (2009) 1417–1426.
[26] M.J. Mitton-Fry, S.J. Brickner, J.C. Hamel, L. Brennan, J.M. Casavant, M. Chen, C. Zook, Novel quinoline derivatives as inhibitors of bacterial DNA gyrase and topoisomerase IV, Bioorg. Med. Chem. Lett. 23 (10) (2013) 2955–2961.
[27] Y. Wang, F. Xiao, G. Jin, Structural basis of quinolone derivatives, inhibition of type I and II topoisomerases and inquiry into the relevance of bioactivity in odd or even branches with molecular docking study, J. Mol. Struct. 1221 (2020) 128869.
[28] S. Picard, G. Clermont, E. Genin, M. Blanchard-Desce, 8-Br-quinoline derivatives as sensitizers combining two-photon induced fluorescence and singlet oxygen generation, Tetrahedron 71 (7) (2015) 1088–1094.
[29] L.D. Costa, J.A. e Silva, S.M. Fonseca, C.T. Arranja, A.M. Urbano, A.J. Sobral, Photophysical characterization and *in vitro* phototoxicity evaluation of 5,10,15,20-tetra(quinolin-2-yl)porphyrin as a potential sensitizer for photodynamic therapy, Molecules 21 (2016) 439.
[30] I. Maliszewska, A. Zdubek, B. Dziuk, P. Boratyński, Quinine and quinidine derivatives as photosensitizers for photodynamic inactivation of bacterial pathogens, J. Nat. Prod. 88 (8) (2025) 1907–1918.
[31] K. Hiratani, K. Taguchi, H. Sugihara, K. Iio, The synthesis of Li+−selective polyether carriers and thier behavior in cation transport through liquid membranes, Bull. Chem. Soc. Jpn. 57 (7) (1984) 1976–1984.
[32] X. Li, B.D. Zheng, X.H. Peng, S.Z. Li, J.W. Ying, Y. Zhao, J.D. Huang, J. Yoon, Phthalocyanines as medicinal photosensitizers: developments in the last five years, Coord. Chem. Rev. 379 (2019) 147–160.
[33] W. Zhao, L. Wang, M. Zhang, Z. Liu, C. Wu, X. Pan, Z. Huang, C. Lu, G. Quan, Photodynamic therapy for cancer: mechanisms, photosensitizers, nanocarriers, and clinical studies, MedComm 5 (7) (2024) e603.
[34] S. Ünlü, F. Tuncel Elmalı, G. Yaşa Atmaca, A. Erdoğmuş, Synthesis of axially Schiff base new substituted silicon phthalocyanines and investigation of photochemical and sono-photochemical properties, Photodiagnosis Photodyn. Ther. 40 (2022) 103192.
[35] İ. Değirmencioğlu, K. İren, İ. Yalçin, C. Göl, M. Durmuş, Synthesis of axially disubstituted silicon (IV) phthalocyanines and investigation of their photophysical and photochemical properties, J. Mol. Struct. 1249 (2022) 131599.
[36] B. Koca, E. Hamuryudan, S. Catak, A. Erdogmus, A. Monari, V. Aviyente, Exploring the photophysics of polyfluorinated phthalocyanine derivatives as potential theranostic agents, J. Phys. Chem. C 123 (40) (2019) 24417–24425.
[37] G.G. Köse, A novel diaxially silicon phthalocyanine sensitizer for the generation of high efficiency singlet oxygen in photochemical and sono-photochemical studies, J. Organomet. Chem. 998 (2023) 122814.
[38] H. Messaoudi, G.Y. Atmaca, A. Erdoğmuş, Novel axially di-substituted natural, cationic and zwitter ionic silicon phthalocyanine derivatives: synthesis, characterization, sono-photochemical properties, J. Mol. Struct. 1312 (2024) 138394.
[39] G.H. Raab, A.F. Schneider, W. Eiermann, H. Gottschalk-Deponte, R. Baumgartner, W. Beyer, Response of human endometrium and ovarian carcinoma cell lines to photodynamic therapy, Arch. Gynecol. Obstet. 248 (1990) 13–20.
[40] L. Varriale, E. Coppola, M. Quarto, B.M. Veneziani, G. Palumbo, Molecular aspects of photodynamic therapy: low energy pre-sensitization of hypericin-loaded human endometrial carcinoma cells enhances photo-tolerance, alters gene expression and affects the cell cycle, FEBS Lett. 512 (2002) 287–290.
[41] T. Keleş, G. Seyhan, Z. Biyiklioglu, K. Kolci, R. Reis, B. Barut, Dendritic, water-soluble, and nonaggregated axially substituted silicon phthalocyanine as a potential endometrial anticancer agent, Appl. Organomet. Chem. 38 (2024) e7699.
[42] J. Chen, Y. Wang, Y. Fang, Z. Jiang, A. Wang, J. Xue, Improved photodynamic anticancer activity and mechanisms of a promising zinc(II) phthalocyanine-quinoline conjugate photosensitizer *in vitro* and *in vivo*, Biomed. Opt. Express 11 (7) (2020) 3900–3912.
[43] T.N. Soliman, D. Keifenheim, P.J. Parker, D.J. Clarke, Cell cycle responses to topoisomerase II inhibition: molecular mechanisms and clinical implications, J. Cell Biol. 222 (12) (2023) e202209125.
[44] J. Chen, The cell-cycle arrest and apoptotic functions of p53 in tumor initiation and progression, Cold Spring Harb. Perspect. Med. 6 (3) (2016) a026104.
[45] B. Alshehri, Cytochrome c and cancer cell metabolism: a new perspective, Saudi Pharm. J. 32 (12) (2024) 102194.
[46] J.C. Lien, S.Y. Hsu, F.S. Chueh, Y.S. Ma, Y.L. Chu, Y.C. Chou, K.C. Lai, J.C. Chen, Y. P. Huang, R.S. Wu, Newly synthesized PW06 induced cell apoptosis in human glioblastoma multiforme GBM 8401 cells through caspase- and mitochondria-dependent pathways, J. Biochem. Mol. Toxicol. 39 (5) (2025) e70264.
[47] G. Xia, R. Cao, L. Huang, F. Wang, X. Chu, Q. Zhang, R. Wang, J. Piloto-Ferrer, F. Yuan, J. Li, D. Jia, Development of an active loading strategy for methylene blue in liposomes and its application in EGFR-targeted photodynamic therapy, J. Pharm. Sci. 115 (4) (2026) 104213.
[48] Y. Wang, S. Chen, C. Wu, Y. Liao, T. Lin, K. Liu, Y. Chen, T. Li, T. Chien, N. Chan, Producing irreversible topoisomerase II-mediated DNA breaks by site-specific pt (II)-methionine coordination chemistry, Nucleic Acids Res. 45 (2017) 10861–10871.
[49] C.M. Chang, S. Wang, C. Wang, A.H. Pang, C. Yang, Y. Chang, W. Wu, M. Tsai, A unified view on enzyme catalysis by cryo-EM study of a DNA topoisomerase, Commun. Chem. 7 (2024) 10861–10871.

**Gökçe Seyhan** is a research assistant in the Department of Biochemistry at the Faculty of Pharmacy, Karadeniz Technical University, and conducts research in the fields of biochemistry, pharmacology, and photodynamic therapy.

**Yasemin Altun Ali** is a research assistant in the Department of Pharmaceutical Toxicology within the Division of Pharmaceutical Sciences at the Faculty of Pharmacy, Karadeniz Technical University. She completed her undergraduate education at Karadeniz Technical University, obtained her master's degree from Ankara University, and is currently pursuing her PhD at the Faculty of Pharmacy, Istanbul University.

**Elif Nur Barut** is an associate professor at the Faculty of Pharmacy, Karadeniz Technical University, and conducts research in the fields of pharmacology and experimental disease models.

**Manar M. Amin** is a PhD student in the Department of Pharmacology, where she is actively involved in academic and research activities. Her research focuses on pharmacology and experimental disease models.

**Turgut Keles** is a lecturer at Recep Tayyip Erdoğan University and conducts research in the fields of inorganic chemistry and general chemistry.

**Suat Sari** is an associate professor in the Department of Pharmaceutical Chemistry at the Faculty of Pharmacy, Hacettepe University, and conducts research in the fields of medicinal chemistry, molecular modeling, and computer-aided drug design.

**Baybars Koksoy** is an associate professor in the Department of Chemistry at the Faculty of Engineering and Natural Sciences, Bursa Technical University, and conducts research in the fields of organic chemistry, photochemistry, and light-absorbing materials.

**Can Özgür Yalcin** is an associate professor in the Department of Pharmaceutical Toxicology within the Division of Pharmaceutical Sciences at the Faculty of Pharmacy, Karadeniz Technical University, and conducts research in the fields of toxicology, pharmacology, and pharmaceutical toxicology.

**Zekeriya Biyiklioglu** is a professor in the Department of Inorganic Chemistry at the Faculty of Science, Karadeniz Technical University, and focuses on the synthesis of phthalocyanine-based compounds.

**Burak Barut** is an associate professor in the Department of Biochemistry at the Faculty of Pharmacy, Karadeniz Technical University. His research focuses on biochemistry, photodynamic therapy, and the synthesis and biological evaluation of phthalocyanine-based compounds, particularly in relation to anticancer applications.